# Benchmarking Perovskite Electrocatalysts' OER Activity as Candidate Materials for Industrial Alkaline Water Electrolysis

**DJ Donn Matienzo** [1,2,*], **Tuğçe Kutlusoy** [3], **Spyridon Divanis** [3], **Chiara Di Bari** [1] **and Emanuele Instuli** [1,*]

[1] New Application Research, Research and Development Division, Industrie De Nora S.p.A., 20134 Milan, Italy; chiara.dibari@denora.com

[2] Department of Inorganic Technology, University of Chemistry and Technology, Technická 5, 166 28 Prague 6, Czech Republic

[3] Center of Excellence (CoE), Department of Chemistry, University of Copenhagen, Universitetsparken 5, 2100 København Ø, Copenhagen, Denmark; tuk@chem.ku.dk (T.K.); spiros@chem.ku.dk (S.D.)

\* Correspondence: djdonn.matienzo@denora.com or matienzd@vscht.cz (D.D.M.); emanuele.instuli@denora.com (E.I.); Tel.: +39-02-2129-2124 (D.D.M.)

check for updates

**Abstract:** The selection and evaluation of electrocatalysts as candidate materials for industrial alkaline water electrolysis is fundamental in the development of promising energy storage and sustainable fuels for future energy infrastructure. However, the oxygen evolution reaction (OER) activities of various electrocatalysts already reported in previous studies are not standardized. This work reports on the use of perovskite materials ($LaFeO_3$, $LaCoO_3$, $LaNiO_3$, $PrCoO_3$, $Pr_{0.8}Sr_{0.2}CoO_3$, and $Pr_{0.8}Ba_{0.2}CoO_3$) as OER electrocatalysts for alkaline water electrolysis. A facile co-precipitation technique with subsequent thermal annealing (at 700 °C in air) was performed. Industrial requirements and criteria (cost and ease of scaling up) were well-considered for the selection of the materials. The highest OER activity was observed in $LaNiO_3$ among the La-based perovskites, and in $Pr_{0.8}Sr_{0.2}CoO_3$ among the Pr-based perovskites. Moreover, the formation of double perovskites ($Pr_{0.8}Sr_{0.2}CoO_3$ and $Pr_{0.8}Ba_{0.2}CoO_3$) improved the OER activity of $PrCoO_3$. This work highlights that the simple characterization and electrochemical tests performed are considered the initial step in evaluating candidate catalyst materials to be used for industrial alkaline water electrolysis.

**Keywords:** perovskites; oxygen evolution reaction; alkaline water electrolysis; electrocatalysts

## 1. Introduction

Hydrogen could play a huge role in energy transition and in reaching transportation and climate objectives, eliminating problems created by fossil fuels [1]. The use of hydrogen has two major roles in decarbonizing major sectors of the economy and can be broadly categorized into either: (a) as a feedstock; or (b) as an energy vector that could enable energy transition [2]. However, over 95% of current hydrogen production is still fossil fuel-based. Steam-methane reforming (SMR) is the most common method of producing hydrogen due to its cost-effectivity. Other processes, such as oil and coal gasification, are also widely used, particularly in China and Australia. Only around 4% of the global hydrogen supply is produced via electrolysis [3]. This presents the major problem of using fossil fuels, which creates a significant amount of greenhouse gas (GHG) emissions. Therefore, a shift in hydrogen production via electrolysis has an extremely large potential to reduce GHG emissions as well as provide energy storage and sustainable fuels for future energy infrastructure.

The process of water electrolysis breaks down water into hydrogen and oxygen by using electricity. Ideally, the electrical energy needed for electrolysis should come from renewable sources to make the overall process sustainable. Using water electrolysis offers some advantages: (a) the produced hydrogen is pure; (b) the hydrogen is produced directly at the location of use and does not need to be stored; (c) it provides a cheaper alternative compared to when gas is supplied in high-pressure cylinders [4]. However, water electrolysis is still not optimal because of the sluggish kinetics of the anodic oxygen evolution reaction (OER) due to the well-known scaling relation restriction [5].

Moreover, electrolyzer technologies under development could be categorized according to the type of the electrolyte used: (1) alkaline (basic); (2) polymer electrolyte membrane cells (acidic); (3) solid oxide cells (could work in organic or fossil fuels) [6]. Among these technologies, operation in alkaline conditions offers the possibility of using non-precious metal electrocatalysts [7], cost-efficient cell components, and lower energy consumption. These advantages could lead to the possibility of cheaper hydrogen production [8]. Existing industrial alkaline water electrolysis plants are based on cells with an aqueous KOH or NaOH (20 to 40 wt.%) electrolyte and a porous separator at temperatures between 60 °C and 90 °C and at atmospheric or elevated pressure (up to 30 bar) [9–11]. Nearly 20–30% of the total cost of an alkaline water electrolysis plant comes from the cell and stack costs. With this, an increase in the cell performance is well sought if it is balanced by a small cost increase, which favors non-precious metal materials in commercial water electrolysis cells [8].

Numerous studies [12–14] have already discussed the use of transition metal oxides as the most suitable OER electrode material. Significant interest in perovskites has been shown in the works of Suntivich et al. [15] and by Bockris and Otagawa [16,17]. These materials have an $ABO_3$ structure with rare or alkaline earth cations on the A-site and transition metal cations on the B-site. In addition, this current study explores the OER activity of double perovskite materials—$Pr_xM_{1-x}CoO_3$ (M = Sr or Ba). These catalysts were chosen because, as reported by Grimaud et al. [18], this type of material exhibits OER activities comparable to $Ba_{0.5}Sr_{0.5}Co_{0.8}Fe_{0.2}O_{3-\delta}$ (BSCF), which is the most active cubic perovskite reported. The physical origin of the high activity of these Co-based double perovskites can be explained by having the O *p*-band center neither too close nor too far from the Fermi level as predicted by Density Functional Theory (DFT). Nevertheless, the scope of this study is to support the reported DFT calculation results through experimental works. The effects of forming the double perovskites by combining two metals on the A-site metal on the properties of the materials, and especially on the OER activity, are evaluated in this study.

The industrial requirements and criteria (cost and ease of scaling up) were also well-considered for the selection of the materials. With the developed perovskite materials, the use of noble metals could be eliminated. Lanthanides and transition metals belong to the group of highly abundant metals, which does not cause problems in the purchase of bulk materials for industrialization. Moreover, this type of catalyst synthesis technique also has a great impact on adapting the synthesis from lab-scale (in the order of mg to g in one synthesis batch) to industrial scale (in the order of g to kg in one synthesis batch). The investment cost estimations of an alkaline water electrolysis plant mainly depend on its size and other site-specific characteristics [19,20]. However, from the report released by Bertuccioli et al. [19], the estimated range of 1100 EUR/kW capacity as the central investment cost for 2015 has a large potential for cost reduction down to 580 EUR/kW capacity in 2030. This could be achieved by designing the cell more efficiently as well as by using materials which are economically viable but of a comparable performance with the benchmark catalysts, typically composed of noble metals.

This work reports on the use of perovskite materials ($LaFeO_3$, $LaCoO_3$, $LaNiO_3$, $PrCoO_3$, $Pr_{0.8}Sr_{0.2}CoO_3$, and $Pr_{0.8}Ba_{0.2}CoO_3$) as OER electrocatalysts for alkaline water electrolysis. A facile co-precipitation technique with subsequent thermal annealing (at 700 °C in air) was performed to synthesize the studied materials. The overall objective of this work is to benchmark various perovskite electrocatalysts by evaluating their material properties, especially OER activity in alkaline media. The developed benchmarking procedure in this work provides an easy strategy that could help in screening a wide number of catalysts to be used in OER for industrial alkaline water electrolysis.

## 2. Results and Discussion

### 2.1. Structural and Morphological Analysis

The crystalline phases of the prepared perovskite materials by co-precipitation method with subsequent calcination at 700 °C were analyzed by XRD (Figure 1). The vertical lines mark the positions of individual reflections of standard cubic $LaFeO_3$ (ICDD No. 04-013-9870), hexagonal $La_2O_3$ (04-015-4999), rhombohedral $LaCoO_3$ (04-015-9698), rhombohedral $LaNiO_3$ (04-013-6811), ortho-rhombic $PrCoO_3$ (04-013-4301), orthorhombic $Pr_{0.8}Sr_{0.2}CoO_3$ (04-008-6534), and orthorhombic $Pr_{0.8}Ba_{0.2}CoO_3$ (04-015-0639). It can be noted that, apart from the $LaFeO_3$ sample (with $La_2O_3$ impurity), there are no other impurities present (i.e., metal oxides or hydroxides) on the materials developed.
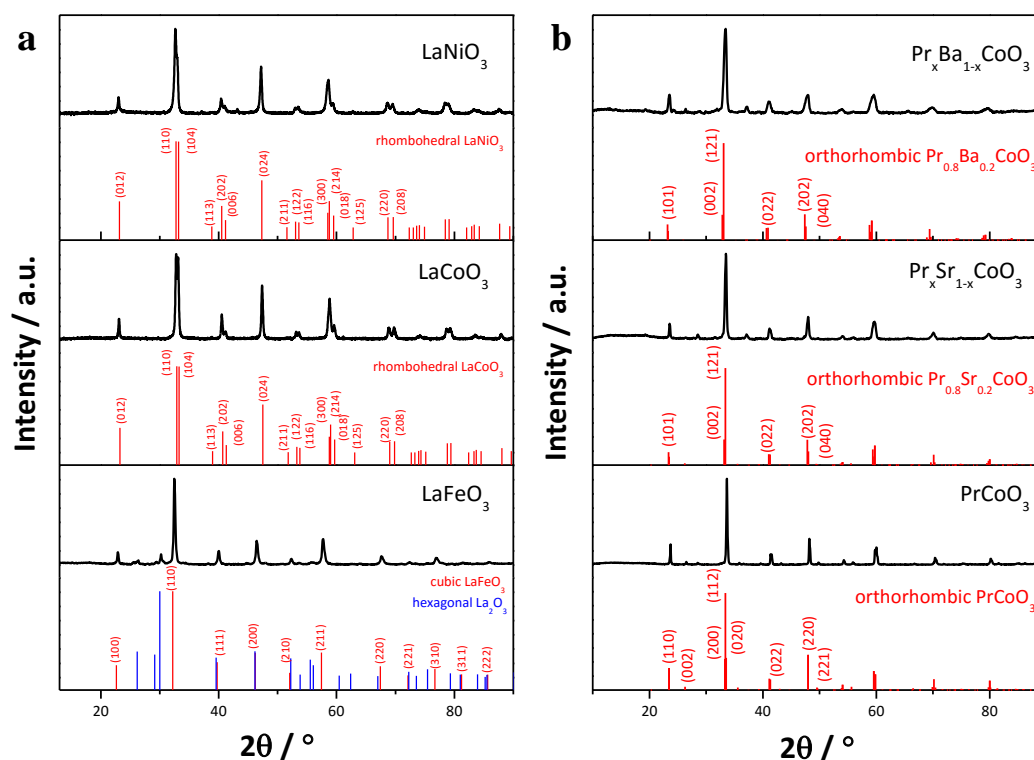


**Figure 1.** Powder XRD patterns of (**a**) $LaFeO_3$, $LaCoO_3$, $LaNiO_3$; (**b**) $PrCoO_3$, $Pr_xSr_{1-x}CoO_3$, $Pr_xBa_{1-x}CoO_3$ precursors prepared by the co-precipitation technique with subsequent calcination at 700 °C in air.

Rietveld refinement of the experimental diffraction patterns was performed, and the results of the analysis are summarized in Table 1 (for more details, see Figure S1). In this particular case, the Rietveld refinement is useful for quantifying the amount the $La_2O_3$ impurities present in the $LaFeO_3$ sample. The results show that around 9.8% hexagonal $La_2O_3$ is present in the sample. In addition, the results from the full Rietveld refinement show the formation of phase-pure orthorhombic $Pr_{0.8}Sr_{0.2}CoO_3$ and $Pr_{0.8}Ba_{0.2}CoO_3$. However, this is not consistent with the equimolar amounts of the A-site metals (Pr and Sr; Pr and Ba) initially added for the preparation of the materials. In this case, the theoretical composition of the double perovskites is $Pr_{0.5}Sr_{0.5}CoO_3$ and $Pr_{0.5}Ba_{0.5}CoO_3$. To verify the Rietveld refinement results, energy-dispersive X-ray spectroscopy (EDX) analysis was performed (see Table S1). The chemical composition analysis obtained from EDX confirms that Sr or Ba are present in 20 at.% of the A-site and Pr is present in 80 at.%. The reason for the formation of non-equimolar A-site metals could be due to the incomplete precipitation of Sr and/or Ba in the initial solution. Residual Sr and/or Ba salts in the supernatant led to the lesser amount of Sr or Ba on the final materials. Optimization of the co-precipitation on these materials could be performed as an extension of this work.

**Table 1.** Rietveld refinement results of XRD patterns for La- and Pr-based perovskites.

| | Space Group | Phase Composition/ vol% | a/Å | b/Å | c/Å | Volume/Å$^3$ | Crystallite Size/nm | $\chi^2$/% |
|---|---|---|---|---|---|---|---|---|
| $LaFeO_3$ | *Pm3m* | 90.2% cubic $LaFeO_3$; 9.8% hexagonal $La_2O_3$ | 3.9300 | 3.9300 | 3.9300 | 60.6988 | 31.4 | 5.33 |
| $LaCoO_3$ | *R-3c* | 100% rhombohedral $LaCoO_3$ | 5.4364 | 5.4364 | 13.1134 | 335.6294 | 58.2 | 2.34 |
| $LaNiO_3$ | *R-3c* | 100% rhombohedral $LaNiO_3$ | 5.4456 | 5.4456 | 13.1443 | 337.5681 | 25.5 | 4.35 |
| $PrCoO_3$ | *Pnma* | 100% orthorhombic $PrCoO_3$ | 5.3459 | 7.5814 | 5.3814 | 218.1059 | 77.1 | 9.88 |
| $Pr_{0.8}Sr_{0.2}CoO_3$ | *Pnma* | 100% orthorhombic $Pr_{0.8}Sr_{0.2}CoO_3$ | 5.3746 | 7.6079 | 5.4193 | 221.5911 | 76.2 | 7.82 |
| $Pr_{0.8}Ba_{0.2}CoO_3$ | *Pnma* | 100% rhombohedral $Pr_{0.8}Sr0._2CoO_3$ | 5.3892 | 7.6155 | 5.4536 | 223.5603 | 67.8 | 5.42 |

Moreover, the calculated unit cell parameters and unit cell volume reported in Table 1 are in good agreement with the unit cell parameters of the following standards: (1) cubic $LaFeO_3$ (a = b = c = 3.9286 Å, 60.63 Å$^3$); (2) rhombohedral $LaCoO_3$ (a = b = 5.4390 Å, c = 13.1100 Å, 335.9 Å$^3$); (c) rhombohedral $LaNiO_3$ (a = b = 5.4596 Å, c = 13.1421 Å, 339.3 Å$^3$); (d) orthorhombic $PrCoO_3$ (a = 5.3401 Å, b = 7.5741, c = 5.3750 Å, 217.7 Å$^3$). For the double perovskites ($Pr_{0.8}Sr_{0.2}CoO_3$ and $Pr_{0.8}Ba_{0.2}CoO_3$), the lattice parameters and unit cell volume of $PrCoO_3$ increased. This signifies the insertion of $Sr^{2+}$ and/or $Ba^{2+}$ into the $PrCoO_3$ crystal lattice.

The characteristic particle sizes obtained from the SEM images of the materials are shown in Figure 2. The calcination temperature employed in the preparation of the materials clearly affects the resulting perovskite catalyst particle sizes. In this case, the nanosized character is lost, thus obtaining particle sizes in the micron scale range (ca. 180 to 230 nm). Additionally, it can also be observed from the SEM images that the particles of the prepared materials show isometric shape without preferential surface orientation. As mentioned earlier, the chemical compositions were evaluated by EDX analysis (see Table S1). The results show that the chemical compositions match the projected ratios of lanthanum and B-site metal cations in the starting solutions. In the XRD analysis, the formation of crystalline $La_2O_3$ was observed in $LaFeO_3$. In the material preparation, an equimolar amount of La and Fe was added; therefore, iron-containing species (iron oxide and/or iron hydroxide) should also be present in the $LaFeO_3$ materials, which was confirmed by EDX analysis. The results show that A and B metal cations are present in almost the same at.%. The Fe-containing species, which were not detected by XRD analysis, suggest that these material components could be amorphous or present in a very low amount.
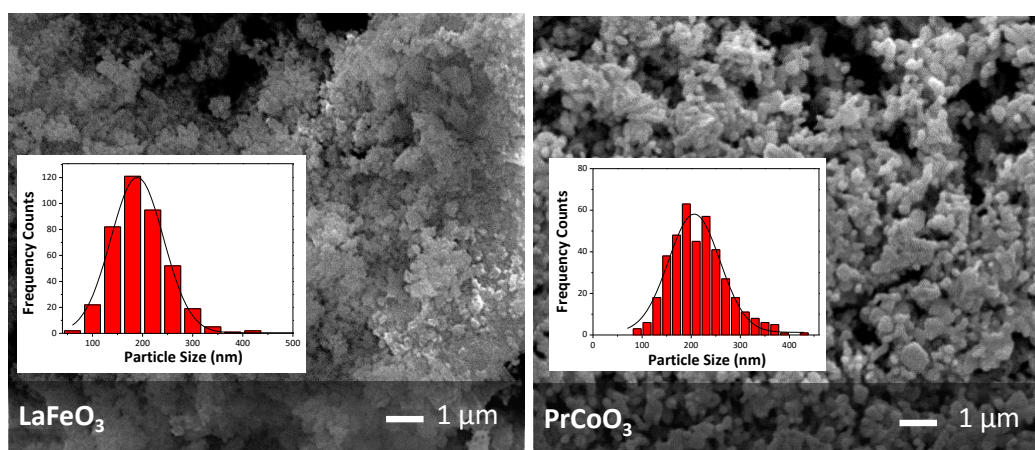


**Figure 2.** *Cont.*
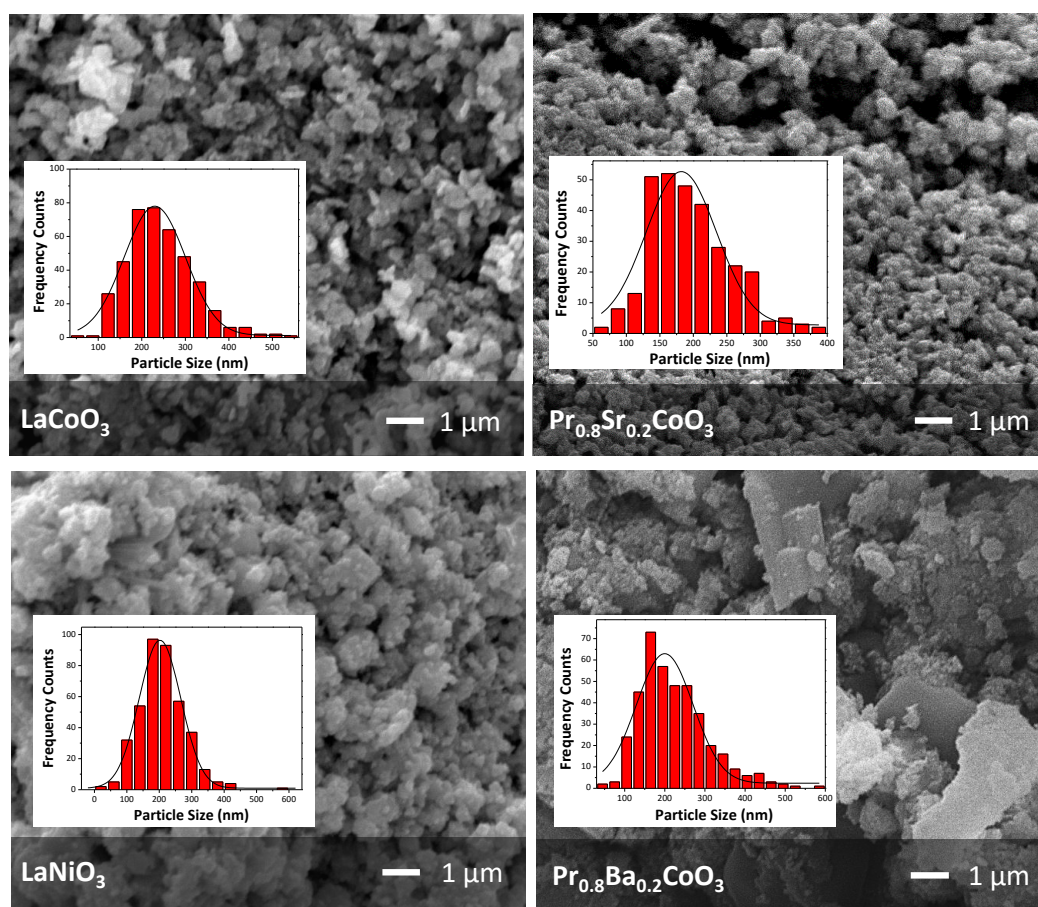
| Sample | Diameter [nm] |
|---|---|
| LaFeO$_3$ | 189 ± 1 |
| LaCoO$_3$ | 230 ± 3 |
| LaNiO$_3$ | 202 ± 2 |
| PrCoO$_3$ | 205 ± 3 |
| Pr$_{0.8}$Sr$_{0.2}$CoO$_3$ | 182 ± 6 |
| Pr$_{0.8}$Ba$_{0.2}$CoO$_3$ | 200 ± 6 |

Statistical analysis of size distribution from 400 particles.

**Figure 2.** SEM images depicting the surface morphologies and particle size distribution of the prepared La- and Pr-based perovskites.

## 2.2. Electrochemical Performance

The cyclic voltammograms and the corresponding Tafel plots of the perovskite materials are shown in Figures 3 and 4, respectively. The Tafel plots are obtained by averaging the currents in the forward and backward scans of the last cycle and subtracting the ohmic losses. For the La-based perovskites, the observed trend in the OER activity (overpotential values at 1 mA cm$^{-2}$, see Figure 5) for different B-site metal cations (highest to lowest activity) is LaNiO$_3$ > LaCoO$_3$ > LaFeO$_3$, confirming the previously reported results by Bockris and Otagawa [17,21]. In this previous report, they proposed a relationship between the electronic structure and the OER activity of the perovskites by using the

bond strength of the surface oxygenated intermediates as a descriptor. They successfully displayed this correlation in a volcano plot of activity in terms of the bond strength (linear relationship with the number of d-electrons). Therefore, $LaNiO_3$ appears at the top of the activity volcano based on the binding energy of HO*. However, at relatively low current densities, the formation of the $NiOOH/Ni(OH)_2$ ($Ni^{3+}/Ni^{2+}$) redox couple could be observed. This is due to the deterioration of the rhombohedral $LaNiO_3$ structure [22,23].
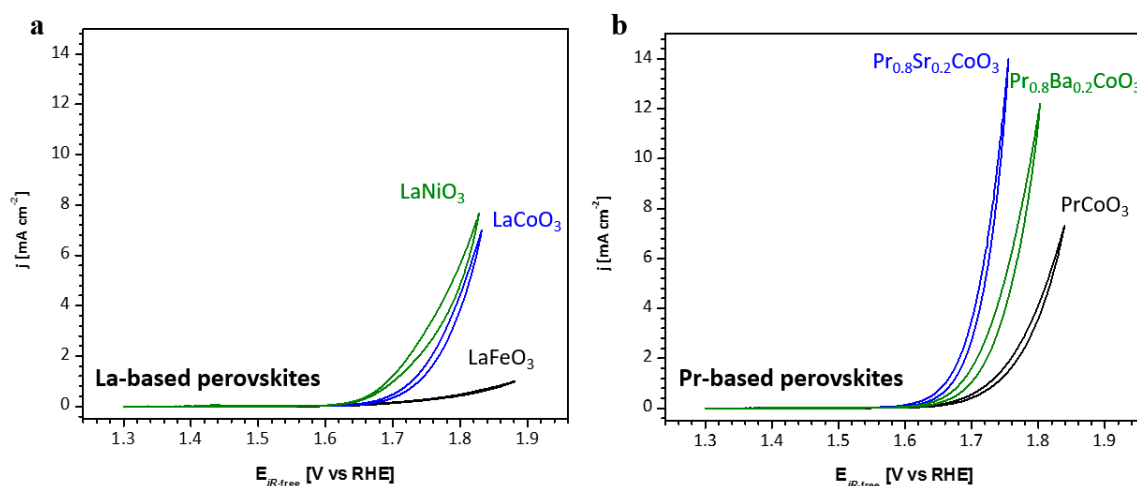


**Figure 3.** Oxygen evolution activities (cyclic voltammograms) of (**a**) La-based perovskites, and (**b**) Pr-based perovskites.
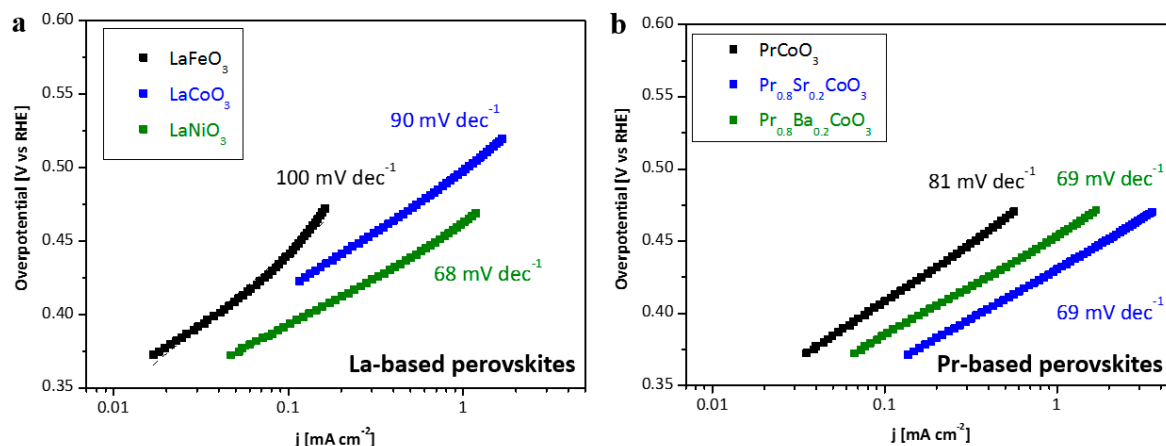


**Figure 4.** Tafel plots of the oxygen evolution obtained from the cyclic voltammograms of (**a**) La-based perovskites, and (**b**) Pr-based perovskites.

The differences in the observed Tafel slope among the La-based perovskites indicate that the OER mechanism is affected by the B-site metal cations. The Tafel slope of ca. 60 mV dec$^{-1}$ ($LaNiO_3$ and $LaCoO_3$) indicates that the rate-determining step is the chemical reaction following the one-electron transfer reaction, while the Tafel slope ca. 120 mV dec$^{-1}$ ($LaFeO_3$) indicates that the first electron transfer reaction is the rate-determining step [24]. Singh et al. [25] reported Tafel slopes of 40 to 65 mV dec$^{-1}$ for $LaNiO_3$, while Lopez et al. [26] reported a Tafel slope of ca. 75 mV dec$^{-1}$ for $LaCoO_3$ obtained by the sol–gel method. Lastly, the high Tafel slope ca. 100 mV dec$^{-1}$ obtained from $LaFeO_3$ is comparable to the values obtained in the lanthanum–calcium ferrites synthesized by the nitrate combustion method [27]. Therefore, the Tafel slopes reported in this study for La-based perovskites are similar or comparable to those reported in previous studies, even if the synthesis technique used was different.

For the Pr-based perovskites, the incorporation of Sr or Ba into the $PrCoO_3$ structure improved the OER activity. The trend of OER activity (overpotential values at 1 mA cm$^{-2}$; see Figure 5) from

highest to lowest is $Pr_{0.8}Sr_{0.2}CoO_3 > Pr_{0.8}Ba_{0.2}CoO_3 > PrCoO_3$. The Tafel slope slightly decreased from ca. 80 mV dec$^{-1}$ for $PrCoO_3$ to 70 mV dec$^{-1}$ for $Pr_{0.8}Sr_{0.2}CoO_3$ and $Pr_{0.8}Ba_{0.2}CoO_3$. These values agree with the reported Tafel slope of Grimaud et al. [18] for the double perovskites obtained by the conventional solid-state route.
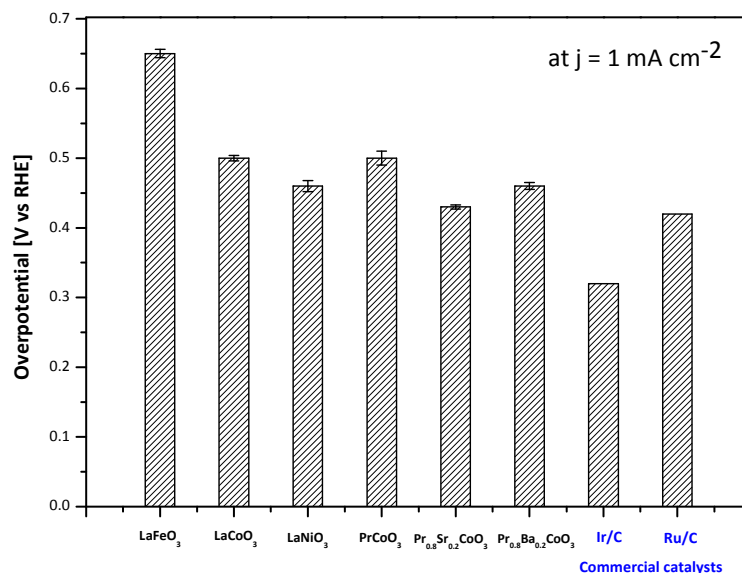


**Figure 5.** Comparison of oxygen evolution reaction (OER) overpotential values (V vs. reversible hydrogen electrode RHE at 1 mA cm$^{-2}$ of the prepared perovskites.

Lastly, the OER activities (overpotential values at 1 mA cm$^{-2}$, see Figure 5) of the synthesized perovskites were compared with commercial Ir and Ru nanoparticles supported on carbon, which are usually used as OER activity benchmark catalysts [28,29]. The results show that the synthesized perovskites ($Pr_{0.8}Sr_{0.2}CoO_3$) have a comparable OER activity to the commercial Ru/C catalysts. This is advantageous in terms of cost since the perovskite electrocatalysts presented do not require the use of noble metals (i.e., Ir and/or Ru), yet they exhibit a comparable performance to the benchmark OER catalysts, leading to an economically viable material for industrial alkaline water electrolysis.

## 3. Materials and Methods

### 3.1. Synthesis of Perovskite Materials

The synthesis of various perovskites ($ABO_3$, A = La, Pr, $Pr_{0.8}Sr_{0.2}$, or $Pr_{0.8}Ba_{0.2}$ and B = Fe, Co, or Ni) was based on the co-precipitation synthesis of $LaMnO_3$ reported by Feng et al. [30]. In this technique, a corresponding stoichiometric amount of A-site metal nitrates ($La(NO_3)_2 \cdot 6H_2O$, $Pr(NO_3)_3 \cdot 6H_2O$, $Sr(NO_3)_2$, or $Ba(NO_3)_2$) and B-site metal nitrates ($Fe(NO_3)_3 \cdot 9H_2O$, $Co(NO_3)_2 \cdot 6H_2O$, or $Ni(NO_3)_2 \cdot 6H_2O$) was dissolved in deionized water. All the reagents were purchased from Sigma-Aldrich and Honeywell Fluka$^{TM}$ (for $Co(NO_3)_2 \cdot 6H_2O$). After stirring at room temperature for at least 1 h (to ensure complete dissolution), KOH solution was dropped in slowly while the solution was continuously stirred. The molar ratio used in this work was A nitrate:B nitrate:KOH = 1:1:6. After stirring for about 10 to 15 min, the formed precipitate was washed with deionized water (until at approximately neutral pH) and was collected using a centrifuge. The filtered precipitate was then dried in air at 60 °C for 3 h. Finally, to obtain the desired perovskite structures, the dried precipitate was calcined at 700 °C for 3 h in air. The samples were then ground into a fine powder to be used for further characterization.

### 3.2. Structural and Morphological Characterization of Perovskite Materials

The phase structure of the materials was determined by performing X-ray diffraction (XRD) analysis using Cu Kα radiation on a Panalytical X'Pert PRO MPD (Multi-Purpose Diffractometer). The crystalline phases were identified by referring to the ICDD (International Center for Diffraction Data) standards. Panalytical X'pert Highscore Plus software was used to perform Rietveld refinement to evaluate the phase composition, unit cell parameters, and crystallite sizes. The surface morphology of the catalyst and the chemical composition analysis were tested by scanning electron microscopy (SEM) FEI Quanta 400. The images obtained by SEM were examined using an image analysis tool, ImageJ, where particle size measurements were performed.

### 3.3. Electrode Preparation and Electrochemical Tests

The oxygen evolution activities of the prepared materials were evaluated in a standard single-compartment three-electrode cell using a rotating disk electrode (RDE) setup from Pine instruments and Autolab potentiostat following the thin-film RDE approach [31]. The catalyst ink was prepared from a suspension of 5 mg of the perovskite powders in a solution mixture consisting of 0.5 mL of Milli-Q water, 2 mL of isopropanol ($C_3H_7OH$), and 10 μL of binder solution (5 wt.% of Nafion®). The mixture was placed in an ultrasonication bath for 30 min. Afterwards, 10 μL of prepared ink was drop casted onto the polished glassy carbon electrode (with a geometric area of 0.196 cm$^2$) for the evaluation of electrochemical performance.

All the electrochemical measurements were performed at room temperature (25 °C), 0.1 M KOH (pH = 13) electrolyte, and 1600 rpm rotation rate. Firstly, 15 full cycle voltammograms (CVs) were recorded in the potential range 1.3 to 1.9 V (vs. RHE) at 50 mV s$^{-1}$ as a pre-conditioning step of the catalyst layer. The oxygen evolution reaction activities were evaluated by recording a series of CV curves in the potential range 1.3 to 1.9 V (vs. RHE) at 5 mV s$^{-1}$. Overpotential values at 1 mA cm$^{-2}$ were then compared to select the candidate materials that will be used in industrial electrode manufacturing. All measured currents were converted to current densities and potentials were corrected for the ohmic-drop measured by the electrochemical impedance spectroscopy (EIS).

### 4. Conclusions

In summary, $ABO_3$ perovskites (A = La, Pr, $Pr_{0.8}Sr_{0.2}$, or $Pr_{0.8}Ba_{0.2}$; B = Fe, Co, or Ni) were prepared via the co-precipitation method. This work introduces an easy strategy to screen electrocatalysts ($LaFeO_3$, $LaCoO_3$, $LaNiO_3$, $PrCoO_3$, $Pr_{0.8}Sr_{0.2}CoO_3$, and $Pr_{0.8}Ba_{0.2}CoO_3$) to be used as candidate anodic materials for industrial alkaline water electrolysis. Structural and morphological analysis followed by electrochemical characterization of the materials is sufficient to select the candidate materials for industrial electrode manufacturing. The highest OER activity was observed in $LaNiO_3$ among the La-based perovskites, and the highest OER activity was observed in $Pr_{0.8}Sr_{0.2}CoO_3$ among the Pr-based perovskites. Additionally, this work verifies that the formation of double perovskites ($Pr_{0.8}Sr_{0.2}CoO_3$ and $Pr_{0.8}Ba_{0.2}CoO_3$) improves the OER activity of $PrCoO_3$.

It is important to note that the scale up of industrial electrodes using the selected catalysts as active materials could introduce other factors (such as substrates used, deposition technique, and conditions, etc.). These factors should be considered, which is out of the scope of the current work. In addition, this work could be extended by evaluating the stability of the materials, because this is one of the most important criteria in developing electrodes for industrial water electrolysis.

Overall, this work highlights that the simple characterization and electrochemical tests performed are the first and most important steps in evaluating candidate catalyst materials to be used for industrial alkaline water electrolysis.

from the EDX analysis. The error enclosed in parenthesis is given as ± 1σ in at.%, Table S2: Comparison of the electrochemical activity of the perovskites in an alkaline environment (0.1 M KOH, room temperature).

## References

1. Cossar, E.; Barnett, A.O.; Seland, F.; Baranova, E.A. The Performance of Nickel and Nickel-Iron Catalysts Evaluated as Anodes in Anion Exchange Membrane Water Electrolysis. *Catalysts* **2019**, *9*, 814. [CrossRef]

2. Hydrogen Council. *How Hydrogen Empowers the Energy Transition*; Hydrogen Council: Brussels, Belgium, 2017.

3. Gielen, D. *Hydrogen from Renewable Power Technology Outlook for the Energy Transition*; International Renewable Energy Agency: Abu Dhabi, UAE, 2018.

4. Spiegel, C. Introduction to Electrolyzers. Available online: https://www.fuelcellstore.com/blog-section/introduction-to-electrolyzers (accessed on 1 June 2020).

5. Man, I.C.; Su, H.; Calle-Vallejo, F.; Hansen, H.A.; Martinez, J.I.; Inoglu, N.G.; Kitchin, J.; Jaramillo, T.F.; Nørskov, J.K.; Rossmeisl, J. Universalin in Oxygen Evolution Electrocatalysis on Oxide Surfaces. *ChemCatChem* **2011**, *3*, 1159–1165. [CrossRef]

6. Sheffield, J.W.; Martin, K.B.; Folkson, R. Electricity and Hydrogen as Energy Vectors for Transportation Vehicles. In *Alternative Fuels and Advanced Vehicle Technologies for Improved Environmental Performance*; Woodhead Publishing: Great Britain, UK, 2014; pp. 117–137.

7. Mergel, J.; Carmo, M.; Fritz, D. Status on Technologies for Hydrogen Production by Water Electrolysis. *Trans. Renew. Energy Syst.* **2013**, 425–450. [CrossRef]

8. Colli, A.N.; Girault, H.H.; Battistel, A. Non-Precious Electrodes for Practical Alkaline Water Electrolysis. *Materials (Basel)* **2019**, *12*, 1336. [CrossRef]

9. Zeng, K.; Zhang, D. Recent Progress in Alkaline Water Electrolysis for Hydrogen Production and Applications. *Prog. Energy Combust. Sci.* **2010**, *36*, 307–326. [CrossRef]

10. Seetharaman, S.; Balaji, R.; Ramya, K.; Dhathathreyan, K.S.; Velan, M. Graphene Oxide Modified Non-Noble Metal Electrode for Alkaline Anion Exchange Membrane Water Electrolyzers. *Int. J. Hydrogen Energy* **2013**, *38*, 14934–14942. [CrossRef]

11. Vermeiren, P.; Adriansens, W.; Moreels, J.P.; Leysen, R. Evaluation of the Zirfon® Separator for Use in Alkaline Water Electrolysis and Ni-H2 Batteries. *Int. J. Hydrogen Energy* **1998**, *23*, 321–324. [CrossRef]

12. Matsumoto, Y.; Sato, E. Electrocatalytic Properties of Transition Metal Oxides for Oxygen Evolution Reaction. *Mater. Chem. Phys.* **1986**, *14*, 397–426. [CrossRef]

13. Hong, W.T.; Risch, M.; Stoerzinger, K.A.; Grimaud, A.; Suntivich, J.; Shao-Horn, Y. Toward the Rational Design of Non-Precious Transition Metal Oxides for Oxygen Electrocatalysis. *Energy Environ. Sci.* **2015**, *8*, 1404–1427. [CrossRef]

14. Burke, M.S.; Enman, L.J.; Batchellor, A.S.; Zou, S.; Boettcher, S.W. Oxygen Evolution Reaction Electrocatalysis on Transition Metal Oxides and (Oxy) Hydroxides: Activity Trends and Design Principles. *Chem. Mater.* **2015**, *27*, 7549–7558. [CrossRef]

15. Suntivich, J.; May, K.J.; Gasteiger, H.A.; Goodenough, J.B.; Shao-Horn, Y. A Perovskite Oxide Optimized for Oxygen Evolution Catalysis from Molecular Orbital Principles. *Science (80-.)* **2011**, *334*, 1383–1385. [CrossRef] [PubMed]

16. Bockris, J.O.; Otagawa, T. The Electrocatalysis of Oxygen Evolution on Perovskites. *J. Electrochem. Soc.* **1984**, *131*, 290. [CrossRef]

17. Bockris, J.O.; Otagawa, T. Mechanism of Oxygen Evolution on Perovskites. *J. Phys. Chem.* **2002**, *87*, 2960–2971. [CrossRef]

18. Grimaud, A.; May, K.J.; Carlton, C.E.; Lee, Y.-L.; Risch, M.; Hong, W.T.; Zhou, J.; Shao-Horn, Y. Double Perovskites as a Family of Highly Active Catalysts for Oxygen Evolution in Alkaline Solution. *Nat. Commun.* **2013**, *4*, 2439. [CrossRef] [PubMed]

19. Bertuccioli, L.; Chan, A.; Hart, D.; Lehner, F.; Madden, B.; Standen, E. *Development of Water Electrolysis in the European Union*; Element Energy: Cambridge, UK, 2014.

20. Shaner, M.R.; Atwater, H.A.; Lewis, N.S.; McFarland, E.W. A Comparative Technoeconomic Analysis of Renewable Hydrogen Production Using Solar Energy. *Energy Environ. Sci.* **2016**, *9*, 2354–2371. [CrossRef]

21. Otagawa, T.; Bockris, J. Lanthanum Nickelate as Electrocatalyst: Oxygen Evolution. *J. Electrochem. Soc.* **1982**, *129*, 2391. [CrossRef]

22. Soares, C.O.; Silva, R.A.; Carvalho, M.D.; Jorge, M.E.M.; Gomes, A.; Rangel, C.M.; da Silva Pereira, M.I. Oxide Loading Effect on the Electrochemical Performance of LaNiO3 Coatings in Alkaline Media. *Electrochim. Acta* **2013**, *89*, 106–113. [CrossRef]

23. Bursell, M.; Pirjamali, M.; Kiros, Y. La0. 6Ca0. 4CoO3, La0. 1Ca0. 9MnO3 and LaNiO3 as Bifunctional Oxygen Electrodes. *Electrochim. Acta* **2002**, *47*, 1651–1660. [CrossRef]

24. Suen, N.-T.; Hung, S.-F.; Quan, Q.; Zhang, N.; Xu, Y.-J.; Chen, H.M. Electrocatalysis for the Oxygen Evolution Reaction: Recent Development and Future Perspectives. *Chem. Soc. Rev.* **2017**, *46*, 337–365. [CrossRef]

25. Singh, R.N.; Bahadur, L.; Pandey, J.P.; Singh, S.P.; Chartier, P.; Poillerat, G. Preparation and Characterization of Thin Films of LaNiO 3 for Anode Application in Alkaline Water Electrolysis. *J. Appl. Electrochem.* **1994**, *24*, 149–156. [CrossRef]

26. Lopez, K.; Park, G.; Sun, H.-J.; An, J.-C.; Eom, S.; Shim, J. Electrochemical Characterizations of LaMO$_3$ (M = Co, Mn, Fe, and Ni) and Partially Substituted LaNi$_x$M$_{1-x}$O$_3$ (X = 0.25 or 0.5) for Oxygen Reduction and Evolution in Alkaline Solution. *J. Appl. Electrochem.* **2015**, *45*, 313–323. [CrossRef]

27. Sankannavar, R.; Sarkar, A. The Electrocatalysis of Oxygen Evolution Reaction on La1-XCaxFeO3-δ Perovskites in Alkaline Solution. *Int. J. Hydrogen Energy* **2018**, *43*, 4682–4690. [CrossRef]

28. Lee, Y.; Suntivich, J.; May, K.J.; Perry, E.E.; Shao-Horn, Y. Synthesis and Activities of Rutile IrO$_2$ and RuO$_2$ Nanoparticles for Oxygen Evolution in Acid and Alkaline Solutions. *J. Phys. Chem. Lett.* **2012**, *3*, 399–404. [CrossRef] [PubMed]

29. Gorlin, Y.; Jaramillo, T.F. A Bifunctional Nonprecious Metal Catalyst for Oxygen Reduction and Water Oxidation. *J. Am. Chem. Soc.* **2010**, *132*, 13612–13614. [CrossRef]

30. Feng, C.H.; Li, Q.S.; Liu, C.M.; Deng, Y.; Guo, L. Synthesis of Perovskite-Type LaMnO$_3$ under Hydrothermal Conditions. In *Materials Science Forum*; Trans Tech Publications: Stafa-Zurich, Switzerland, 2005; Volume 475, pp. 4051–4054.

31. Schmidt, T.J.; Gasteiger, H.A.; Stäb, G.D.; Urban, P.M.; Kolb, D.M.; Behm, R.J. Characterization of High-surface-area Electrocatalysts Using a Rotating Disk Electrode Configuration. *J. Electrochem. Soc.* **1998**, *145*, 2354–2358. [CrossRef]